HHS Public Access

Author manuscript

Nat Chem Biol. Author manuscript; available in PMC 2022 June 30.

Published in final edited form as:

Nat Chem Biol. 2022 March ; 18(3): 305–312. doi:10.1038/s41589-021-00948-7.

Convergent evolution of bacterial ceramide synthesis

Gabriele Stankeviciute[1,2], **Peijun Tang**[3], **Ben Ashley**[3], **Joshua D. Chamberlain**[1], **Matthew E.B. Hansen**[4], **Aimiyah Coleman**[1], **Rachel D'Emilia**[1], **Larina Fu**[1], **Eric C. Mohan**[3], **Hung Nguyen**[1], **Ziqiang Guan**[5,*], **Dominic J. Campopiano**[3,*], **Eric A. Klein**[1,2,6,*]

[1]Center for Computational and Integrative Biology, Rutgers University-Camden, Camden, NJ 08102, USA

[2]Rutgers Center for Lipid Research, Rutgers University, New Brunswick, NJ 08901, USA

[3]East Chem School of Chemistry, University of Edinburgh, Edinburgh EH9 3FJ, United Kingdom

[4]Department of Genetics, Perelman School of Medicine at the University of Pennsylvania, Philadelphia, PA 19104, USA

[5]Department of Biochemistry, Duke University Medical Center, Durham, NC 27710, USA

[6]Biology Department, Rutgers University-Camden, Camden, NJ 08102, USA.

Abstract

The bacterial domain produces numerous types of sphingolipids with various physiological functions. In the human microbiome, commensal and pathogenic bacteria use these lipids to modulate the host inflammatory system. Despite their growing importance, their biosynthetic pathway remains undefined since several key eukaryotic ceramide synthesis enzymes have no bacterial homologue. Here we used genomic and biochemical approaches to identify six proteins comprising the complete pathway for bacterial ceramide synthesis. Bioinformatic analyses revealed the widespread potential for bacterial ceramide synthesis leading to our discovery of the first known Gram-positive species to produce ceramides. Biochemical evidence demonstrated that the bacterial pathway operates in a different order than in eukaryotes. Furthermore, phylogenetic analyses support the hypothesis that the bacterial and eukaryotic ceramide pathways evolved independently.

*Correspondence to: eric.a.klein@rutgers.edu, Dominic.Campopiano@ed.ac.uk, and ziqiang.guan@duke.edu.

Author contributions: G.S. made the mutant and complementation strains for characterizing the synthetic pathway and performed the lipid extractions. P.T., B.A., and E.C.M. purified and characterized the recombinant proteins. J.D.C. cloned and analyzed the *P. buccae* complementation strains. M.E.B.H. and E.A.K. performed the phylogenetic and bioinformatic analyses. E.A.K. acquired the microscopy images. A.C., R.D., L.F., and H.N. performed the transposon screen to isolate ceramide deficient mutants. Z.G. performed the lipid mass spectrometry analyses. G.S., P.T., B.A., Z.G., D.J.C., and E.A.K. designed the experiments, interpreted the data, and wrote the manuscript.

Competing interests: Authors declare no competing interests.

Introduction

Sphingolipids are found ubiquitously in eukaryotes from fungi, to plants, to animals. By contrast, this class of lipids has been identified in only a handful of bacterial taxa[1]. Within this small group of sphingolipid-producing bacteria there is a tremendous variety of acyl chain length and degree of saturation, acyl chain hydroxylation, and lipid headgroups. This structural diversity is paralleled by a wide range of physiological roles for sphingolipids including modulation of host-microbe interactions[2,3], protection from bacteriophage[4], bacterial life cycle and sporulation[5], and microbial predation[6]. Deeper investigations into the mechanistic roles of sphingolipids in bacterial physiology and host-microbe interactions have been hampered by a lack of knowledge of their biosynthetic pathway. Due to their importance in human health and disease[7], it is not surprising that the eukaryotic biosynthesis pathway has been elucidated in tremendous detail[8]. By contrast, bacteria do not appear to have homologous enzymes, except for serine palmitoyltransferase (Spt) which performs the initial conserved step in ceramide synthesis[9,10].

To date, the presence of predicted *spt* genes is the only indication that a bacterial species may synthesize sphingolipids[11]. However, the presence of a predicted Spt alone is not a particularly reliable indicator of sphingolipid production because there is a high degree of similarity between members of the larger family of α-oxoamine synthases that are involved in heme and biotin synthesis. Here, we identified and characterized the remainder of the bacterial ceramide synthetic pathway. We note that during the preparation of this manuscript, the same set of genes were identified in *C. crescentus*[12]. While the independent identification of this biosynthetic pathway corroborates the importance of these genes in ceramide synthesis, our biochemical data suggested a different function for these enzymes than that originally proposed[12]. Furthermore, the elucidation of the bacterial ceramide synthesis pathway enabled us to perform a bioinformatic screen that led to the identification of 17 taxonomic classes, including the first Gram-positive bacteria, with the potential to synthesize sphingolipids. Lipid profiling of one of these Actinobacteria provided the first demonstration of Gram-positive bacterial ceramides, validated our bioinformatic approach, and suggested that bacterial sphingolipid synthesis occurs across a wide range of organisms. Surprisingly, the bacterial enzymes are not phylogenetically related to those in eukaryotes and the biosynthetic steps occur in a different order than in eukaryotes. These findings support the independent evolution of ceramide production in bacteria and eukaryotes.

Results

Characterization of serine palmitoyltransferase (Spt)

The first step in *de novo* ceramide synthesis, which is conserved between eukaryotes and prokaryotes, is the decarboxylative, Claisen-like condensation of palmitoyl-coenzyme A (palmitoyl-CoA) and L-serine into 3-ketosphinghanine (3-KDS, **1**) (Fig. 1a)[13]. In *C. crescentus*, we previously identified *ccna_01220* as a putative Spt since the Δ*ccna_01220* strain had no detectable ceramide[4]. His-tagged recombinant CCNA_01220 was purified from *E. coli* (see Extended Data Fig. 1a-b); it displayed Spt activity, and the production of 3-KDS was detected by matrix-assisted laser desorption ionization mass spectrometry (MALDI-MS) (Fig. 1b). Kinetic analyses yielded K_m values of 110.40 ± 13.37 μM and 2.98

± 0.25 mM for C16:0-CoA and L-serine, respectively (Fig. 1c), which are comparable to the values determined for *Sphingomonas paucimobilis* and human Spt[14-16]. *C. crescentus* Spt also condensed serine and C16:1-CoA with similar kinetic parameters (see Extended Data Fig. 1c-d). Liquid chromatography/electrospray ionization-tandem mass spectrometry (LC/ESI-MS/MS) analysis of the ceramide molecule from *C. crescentus* showed that C16:0 was preferentially used as the Spt substrate to form the long-chain base (see Extended Data Fig. 1e). In some organisms, such as the gut commensal *Bacteroides thetaiotaomicron*, 1-deoxysphingolipids can be detected when Spt uses alanine as a substrate rather than serine[2]. Similarly, a *C. crescentus* serine auxotroph (Δ*serA*), produced 1-deoxyceramide (see Extended Data Fig. 1f-g).

Genetic screen identifies the ceramide synthesis pathway

In the absence of ceramides, *C. crescentus* becomes resistant to the cationic antimicrobial peptide, polymyxin B (PMX) and increasingly sensitive to bacteriophage Φcr30[4]. Using these two phenotypes of ceramide depletion, we performed a transposon mutagenesis screen incorporating both positive and negative selection to identify candidate genes involved in ceramide synthesis (see Extended Data Fig. 2A, detailed in Materials and Methods). Transposon insertions in cells displaying both selection phenotypes were mapped (see Supplementary Table 1 and Extended Data Fig. 2b) and multiple insertions were found in the *spt* gene validating this approach. These transposon mutants served as a platform for identifying ceramide synthesis enzymes as described below.

Spt enzymes vary in their preferred acyl-CoA substrate; some enzymes utilize fatty acyl-CoA thioesters whereas others use an acyl-chain bound as a thioester to an acyl carrier protein (ACP). Our genetic screening identified *ccna_01223*, a putative acyl-CoA synthetase, which adds CoA to a long-chain fatty acid. Additionally, inspection of neighboring genes revealed a candidate ACP (*ccna_01221*). This genomic arrangement of the Spt, ACP, and ACP-synthetase is similar to that seen in *Sphingomonas wittichii*[17]. Although no transposon insertions were identified in *ccna_01221*, this was not surprising given that the gene is only 261 bp and would therefore have a low probability of containing an insertion. Deletion of either gene resulted in a total loss of ceramides (see Extended Data Fig. 3a-b) and both deletions could be complemented by ectopic expression of the respective gene (see Extended Data Fig. 3a-b). Total ion and extracted ion chromatograms confirm that the deletions did not disrupt global lipid production (see Extended Data Fig. 3c-d and Supplementary Table 3).

In eukaryotes, the second synthetic step is the reduction of 3-KDS to sphinganine (**2**), which is catalyzed by a NADPH-dependent 3-ketodihydrosphinghanine reductase (KDSR) (Fig. 1a). Among our transposon insertions, *ccna_01222* was annotated as an NADH ubiquinone-oxidoreductase. Deletion of *ccna_01222* resulted in a ceramide molecule with a mass reduction of 2 Da (Fig. 2a), corresponding to a loss of two hydrogens. Tandem mass spectrometry (MS/MS) analysis confirmed the retention of the oxidized double bond on the 3-KDS derived sphingoid base (see Extended Data Fig. 4). Complementation of the *ccna_01222* deletion restored ceramide reduction (Fig. 2a). These data suggest that the bacterial reductase acts after the second acyl chain is added to 3-KDS. This contrasts with

the eukaryotic pathway where deletion of KDSR generally leads to an accumulation of 3-KDS substrate and prevents downstream reactions[18]. There have been reports of 3-KDS being acylated directly by ceramide synthase in eukaryotic cells; however, this was only observed when Spt was highly overexpressed and cells were provided with excess serine and palmitate[19]. Since the bacterial reductase uses oxidized ceramide (oxCer) as a substrate, we have named CCNA_01222 Ceramide Reductase (CerR).

In eukaryotes, the second acyl chain is attached to the sphingoid backbone by ceramide synthase (CerS) to form dihydroceramide (**4**) (Fig. 1a). Analysis of our transposon hits pointed to *ccna_01212* as a potential CerS. In *C. crescentus*, this gene is annotated as a dATP pyrophosphohydrolase; however, closely related genes identified by BLAST have a variety of annotations including Gcn5-related N-acetyltransferase (GNAT). Deletion of *ccna_01212* led to a complete loss of ceramides (Fig. 2b), consistent with its role in ceramide synthesis. To confirm the enzymatic activity of CCNA_01212, recombinant protein purified from *E. coli* (see Extended Data Fig. 5a-b) was incubated with the substrates 3-KDS and palmitoyl-CoA. LC/ESI-MS/MS analysis of the reaction product identified the expected ceramide molecule (Fig. 2c). Kinetic analyses showed that CCNA_01212 constitutively hydrolyzed acyl-CoA even in the absence of 3-KDS, and the reaction exhibits substrate inhibition (see Extended Data Fig. 5c). Upon the addition of 3-KDS, the reaction proceeded according to Michaelis-Menten kinetics and we determined the $K_{m,app}$ for C16:0-CoA to be 21.3 ± 4.1 μM (see Extended Data Fig. 5c). Based on these data we have named CCNA_01212 bacterial Ceramide Synthase (bCerS). Since eukaryotic CerS enzymes have specific acyl-chain specificities[20], we assessed the substrate preference of *C. crescentus* bCerS. Recombinant bCerS was incubated with 3-KDS and an equimolar mixture of acyl-CoA substrates ranging from C8-C24, and the relative amount of the respective products was monitored by LC/ESI-MS. *C. crescentus* had the highest *in vitro* activity with C14 and showed very little activity with acyl-CoA thioesters of 18 carbons or longer (see Extended Data Fig. 5d). *In vivo*, the C16 ceramide product is most abundant rather than C14 (see Extended Data Fig. 1e); this may reflect the fact that C16 accounts for 30% of the fatty acid content of the cell, whereas C14 is only 2%[21]. Our experiments demonstrating bCerS activity with acyl-CoA as a substrate are consistent with ceramide synthase activity; however, given that the acyl-CoA is readily hydrolyzed by bCerS to a free fatty acid, we cannot rule out the possibility that bCerS ligates the fatty acid to 3-KDS via a reverse-ceramidase-like mechanism[22].

A common ceramide modification found in fungi, plants, some animal tissues, and bacteria is the addition of a hydroxyl group to form phytoceramides (**6**) (Fig. 1a). In plants, sphingoid base hydroxylase 1/2 (Sbh1/2) adds a hydroxyl group to sphinganine to form phytosphingosine (**3**) prior to the addition of the second acyl chain[23]. In mammals, DES2 has dual Δ^4-desaturase and C-4 hydroxylase activities enabling the hydroxylation of ceramide (**5**) to phytoceramide[24]. *C. crescentus* does not have a homologue of Sbh1/2; DES2 has some homology to the fatty acid desaturase CCNA_03535, though deletion of *ccna_03535* did not abolish ceramide hydroxylation. We did not identify any putative hydroxylases in our transposon screen; however, we hypothesized that this modification may not have a strong effect on one or both of our selection phenotypes. To focus on genes that

promoted PMX-resistance only, we searched the Fitness Browser database[25] and found that the disruption of *ccna_00202*, a DesA-family fatty acid desaturase/hydroxylase, results in PMX resistance. Deletion of *ccna_00202* led to a ceramide molecule with a mass reduction of 16 Da corresponding to the loss of a hydroxyl group (Fig. 2d). Complementation of *ccna_00202* restored ceramide hydroxylation (Fig. 2d). Tandem MS/MS data are consistent with the hydroxylation occurring on C2 of the acyl chain (see Extended Data Fig. 4). For this reason, we have named CCNA_00202 Ceramide Hydroxylase (CerH). Examination of the mass spectra of the CerR deletion mutant showed that hydroxylation remains in the absence of reduction (Fig. 2a). Mechanistically, this suggests that CerH can use either DHC or oxCer as a substrate, or that acyl chain hydroxylation occurs upstream of oxCer reduction.

The ceramide in *C. crescentus* has a monounsaturated acyl chain (see Extended Data Fig. 1e). Acyl chain desaturation has also been reported in *Sphingomonas* species[26]. Attempts to identify a desaturase were unsuccessful. *C. crescentus* encodes at least four DesA-family desaturases (*ccna_00203*, *ccna_01515*, *ccna_01743*, and *ccna_03535*). Deletion of each of these genes individually or in combination had no effect on ceramides. While there could be other, yet unidentified, desaturases, we hypothesized that *C. crescentus* bCerS may have a preference for monounsaturated acyl-CoA substrates. *In vitro*, recombinant bCerS had a 3-fold greater preference for C16:1-CoA over C16:0-CoA as a substrate (see Extended Data Fig. 5e); the saturated and monounsaturated C16 fatty acids are present in equal amounts *in vivo*[21]. *C. crescentus* encodes two orthologues each of FabA/FabB which are involved in the synthesis of monounsaturated fatty acids[27]. These four genes are all essential[28] which precluded direct tests of our hypothesis. Since many bacteria produce fully saturated ceramides[2,5], it appears that this modification is not a universal feature of bacterial ceramide synthesis.

The observations of oxCer in the Δ*cerR* strain (Fig. 2a) and the ability of bCerS to use 3-KDS as a substrate (Fig. 2c) suggested that the order of the synthetic pathway in bacteria is different than that in eukaryotes. Based on the MS data, we can propose the following model for bacterial ceramide synthesis (Fig. 2e). Spt condenses serine with an acyl-thioester (either acyl-ACP or acyl-CoA) to produce 3-KDS. bCerS uses 3-KDS and a second palmitoyl-CoA to generate oxCer which is subsequently reduced to ceramide by CerR. We considered the possibility that CerR may work upstream of bCerS, as in eukaryotes. In this case, an alternative model is that bCerS can use either 3-KDS or sphinganine as a substrate leading to oxCer or ceramide as the final product, respectively. *In vitro* assays using recombinant bCerS show that the enzyme can use either substrate (Fig. 2c and Extended Data Fig. 5f). To determine which pathway was more likely to occur *in vivo*, we used fluorescently tagged proteins to infer the subcellular localization of the synthetic enzymes. Incubation of bacteria with chloroform-saturated Tris buffer results in the preferential permeabilization of the outer membrane and leakage of soluble periplasmic proteins[29] (Fig. 2f). Using this approach with the three core ceramide synthesis genes showed that Spt and bCerS retained fluorescence while the CerR signal was entirely lost (Fig. 2f). Consistent with the purification of recombinant Spt and bCerS as soluble proteins, these imaging studies suggest that Spt and bCerS are cytoplasmic whereas CerR is a soluble periplasmic protein. Though we cannot rule out other mechanisms, the spatial separation of these proteins *in vivo* is consistent with our model in which bCerS acts upstream of CerR (Fig. 2e).

Bacterial ceramides can be modified in a variety of species-specific manners including fatty acid hydroxylation (Fig. 2d), acyl chain branching[2], and head group modification by phosphorylation[2] or glycosylation[4]. In *C. crescentus*, we previously identified two sphingolipid glycosyltransferases[4] and here we report the discovery of a ceramide hydroxylase CerH (Fig. 2d).

Bioinformatic identification of ceramide producing species

The identification of Spt, bCerS, and CerR as the core bacterial ceramide synthetic enzymes in *C. crescentus* presented the opportunity to find orthologues in other species and perform a bioinformatic screen for additional potential ceramide producers. Sphingolipids have been isolated from the oral pathogen *Porphyromonas gingivalis*[3]. The *spt* gene (*pgn_1721*) has been identified[3] and BLAST analysis of bCerS and CerR suggested that PGN_0374 and PGN_1886 are the respective orthologues despite having limited homology (PGN_0374: 25% identical, 43% similar; PGN_1886: 23% identical, 43% similar). Additionally, unlike in *C. crescentus*, the proposed *P. gingivalis* genes are not in the same genomic locus. To test their functionality, we complemented *C. crescentus* deletion strains with the corresponding *P. gingivalis* genes. Complementation with *spt* (*pgn_1721*)[30] yielded both the expected *C. crescentus* ceramide (m/z 588.465 Da) as well as a ceramide with two additional methylene units (m/z 614.478 Da) (Fig. 3a). These data are consistent with previous studies showing that *P. gingivalis* has a substrate preference for 17, 18, and 19-carbon fatty-acyl-CoA substrates[31].

Complementation of Δ*bcerS* with *pgn_0374* restored ceramide synthesis (Fig. 3b); a variety of ceramide molecules were observed suggesting that, like Spt, the *P. gingivalis* bCerS has different substrate preferences than the *C. crescentus* orthologue. Lastly, *P. gingivalis cerR* (*pgn_1886*) was able to rescue ceramide reduction (Fig. 3c). Together, these results demonstrate that screening for organisms with this set of genes could yield a broader set of bacteria with the potential to synthesize ceramides.

A BLAST analysis of Spt, bCerS and CerR against the NCBI prokaryotic representative genomes database (5,700+ representative bacterial organisms; see Materials and Methods and Supplementary Data 1 for detailed search parameters and E-value cutoffs) identified 272 organisms, belonging to 17 taxonomic classes, containing orthologues of all three genes (Fig. 3d, Supplementary Data 1, and Extended Data Fig. 6). Analysis of the distance between these core genes showed that, in most clades, the genes were within 10 kb of one another (see Extended Data Fig. 7a). However, among the Bacteroides these genes were found scattered throughout the genome (see Extended Data Fig. 7a); this is consistent with the high degree of chromosomal plasticity and genomic rearrangements associated with these organisms[32]. Whereas all previously identified ceramide producers are Gram-negative organisms, our bioinformatic analysis suggested that several Gram-positive Actinobacteria may be competent for ceramide synthesis. Lipidomic analyses confirmed the presence of dihydroceramide in *Streptomyces aurantiacus*, providing the first evidence of ceramide lipids in Gram-positive bacteria (Fig. 3e). MS/MS analysis of *S. aurantiacus* showed that, in contrast to *C. crescentus*, fatty acid desaturation occurred on the long-chain base (LCB) (see Extended Data Fig. 7b). Based on phylogenetic clustering of the individual ceramide

synthesis genes (Extended Data Fig. 6), as well as the fact that the three genes are found in a putative operon, it is possible that the ceramide synthesis cassette may have been acquired in these Actinobacteria by horizontal gene transfer from Deltaproteobacteria.

In eukaryotes, organisms often have multiple CerS isoforms with distinct fatty acyl-CoA specificities. For example, the six human CerS isoforms enable the synthesis of ceramides with acyl chain lengths of 14-26 carbons[20]. We performed a bioinformatic search to identify bacterial species with multiple bCerS isoforms and found 22 candidates among the Alphaproteobacteria, Bacteroidia, Balneolia, Chitinophagia, and Rhodothermia (see Supplementary Data 2). In most cases, the two bCerS homologues were far apart on the chromosome making it impossible to know whether the two proteins were truly bCerS isoforms or simply similar N-acetyltransferases. One exception was *Prevotella buccae*, where the two candidate *bcerS* genes were encoded immediately next to one another (HMPREF0649_00885 and HMPREF0649_00886; 57% identical and 74% similar). We complemented the *C. crescentus* Δ*bcerS* strain with each of the *P. buccae* isoforms and found that while both could rescue ceramide synthesis, each enzyme produced distinct lipid products (Fig. 3f). HMPREF0649_00885 preferred a fully saturated LCB substrate while HMPREF0649_00886 used a desaturated LCB (see Extended Data Fig. 7c-d).

Independent evolution of ceramide production in bacteria

While the Spt enzyme catalytic residues are conserved between eukaryotic and bacterial species (see Extended Data Fig. 8), neither CerR nor bCerS share obvious homology to KDSR or CerS, respectively. The closest eukaryotic homologue to CerR is NADH dehydrogenase 1A subcomplex subunit 9 (NDUF9A), which is a component of Complex I in the mitochondrial oxidative phosphorylation pathway. Conversely, the bacterial relatives of KDSR are annotated as short-chain dehydrogenases[33]. While both reductase families have conserved catalytic and NAD-binding sites[34] (see Extended Data Fig. 9), human KDSR and *C. crescentus* CerR are only 27% similar and 14% identical. Phylogenetic clustering of these proteins showed that CerR evolved its ceramide reductase activity convergently, arising from NDUF9A-related genes (Fig. 4a).

Similarly, bCerS is a member of the GNAT family of acyltransferases. Bacteria have a variety of GNAT proteins which are closely related to eukaryotic Gcn5 acyltransferases. Phylogenetic analysis demonstrated that bCerS is a subgroup of bacterial GNATs whereas the eukaryotic CerS is only distantly related to Gcn5 family proteins (Fig. 4b). Indeed, eukaryotic CerS has a highly conserved Lag1P domain[35,36] which is not found in any of the bCerS proteins (see Extended Data Fig. 10). These phylogenetic analyses, coupled with the proposed reordering of the synthetic pathway (Fig. 1a and 2f-g), demonstrate that ceramide synthesis evolved independently in bacteria and eukaryotes.

Discussion

Since the discovery of sphingolipids in the late 19th century by Johann L.W. Thudichum, thousands of publications have demonstrated these lipids to be ubiquitous throughout Eukarya; to date, there are over 500 published headgroup variants and acyl chain modifications among this lipid group (LIPID MAPS,[37]). The diversity of sphingolipids

reflects the multifunctional roles of these molecules: the sphingoid backbone provides structural integrity to the cell membrane, the headgroups are involved in lipid-mediated interactions, and some sphingolipid-derivatives function as intracellular second messengers[7].

The list of bacterial sphingolipid-producing species is comparatively short but growing. Their presence in several taxa begs the question of 'how widespread could this lipid be?'. Our results identify the key enzymes required for bacterial ceramide synthesis. While the Spt enzyme is homologous between prokaryotes and eukaryotes, bCerS and CerR are unique to bacteria. We note a recent publication also identified these genes as being involved in ceramide synthesis in *C. crescentus*[12]. The authors proposed, without direct evidence, that these proteins carry out the same functions as their eukaryotic counterparts (see Reference [12], Figure 11). However, our biochemical analyses demonstrate that CerR and bCerS have unique enzymatic activities and the sequence of synthetic reactions in the bacterial pathway is likely different than that in eukaryotes (Fig. 1a and 2f). The previous findings regarding bacterial ceramide synthesis are actually consistent with our proposed pathway; their thin-layer chromatography (TLC) analysis of the CerR deletion yielded an unidentified band which is likely oxCer (see Reference [12], Figure 9, Δ1164, top-most band). Additionally, ectopic expression of Spt and CerR in *E. coli* did not yield sphinganine, while expression of Spt and bCerS did lead to the production of the fast migrating sphingolipid species (see Reference [12], Supplementary Figure 4). As this molecule does not occur in eukaryotes, they lacked a TLC standard to confirm the identity of this band leading to a challenge in interpreting the data.

Though our data support a mechanism in which bCerS directly adds an acyl chain to 3-KDS, we note that the metabolic intermediate sphinganine has been detected in *B. thetaiotaomicron*[2]. We have tried several lipid extraction methods as well as stable-isotope labeling but have never detected sphinganine in *C. crescentus*. While it is possible that the ceramide synthesis pathway operates differently in *Bacteroides*, given the conservation of this enzyme as well as the ability of the *P. gingivalis* enzyme to complement the deletion in *C. crescentus* that seems less likely. An alternative hypothesis is that *Bacteroides* has a ceramidase enzyme, which is lacking in *C. crescentus*, that hydrolyzes ceramide to sphinganine. Indeed, a bioinformatic search identified two linear amide CN-hydrolases (pfam PF02275; of which ceramidases are members) in *B. thetaiotaomicron*. One of these enzymes hydrolyzes bile acids, however, the function of the second homologue is unknown[38]. *C. crescentus* does not have a homologue of these proteins. Additionally, *B. thetaiotaomicron* can assimilate and metabolize sphinganine from the host gut to produce ceramide lipids[39]. Not surprisingly, the details of SL biosynthesis vary in different bacteria and a working hypothesis is that that their environmental niches provide an opportunity for the utilization of particular SL metabolic pathways. Further characterization of the structures and mechanisms of these enzymes will be necessary to elucidate their physiological functions.

Coupled with phylogenetic analysis, our data support a model in which bacterial ceramide synthesis evolved convergently and independently of the eukaryotic pathway. This type of evolution, where identical substrates and products are metabolized by distinct enzymes, is well characterized particularly in plants. For example, 1) gibberellins (tetracyclic diterpenoid

carboxylic acids) are produced by unique enzymes in plants and fungi[40], 2) several independent enzymatic pathways are used to produce caffeine among plant species[41], and 3) the UDP-glucosyltransferases and β-glucosidases used in the synthesis of benzoxazinoids evolved independently in different plant lineages[42]. One potential mechanism for the independent evolution of metabolic pathways is gene duplication and modification of substrate specificity. In the case of bacterial ceramide synthesis, the CerR protein in *C. crescentus* is related to the NDUF9A-domain protein CCNA_03718 (27% identical and 46% similar). In this study, we found that *P. buccae* encodes two bCerS proteins (57% identical and 74% similar) with unique substrate preferences (Fig. 3f).

Phylogenetic analysis of the three ceramide synthetic genes has identified a wide range of Gram-negative, as well as several Gram-positive, species with the potential to produce ceramides. These organisms occupy a range of habitats including aquatic, soil, and within animal hosts. Among the small subset of previously identified ceramide-producing species, these lipids play roles in outer membrane integrity[43], defense against bacteriophage[4], protection against extracellular stress[12], suppression of host inflammation[2], and their production can be developmentally regulated[5]. Furthermore, lipidomic analyses of these organisms has identified a wide range of ceramide species with varying acyl chain length and saturation, acyl chain hydroxylation, and head group glycosylation and phosphorylation; the consequences of these modifications are yet to be determined. By defining the microbial blueprint for ceramide synthesis, we now have a platform for dissecting the physiological functions of these lipids and for potentially engineering the production of novel sphingolipids.

Materials and Methods

Bacterial strains, plasmids, and growth conditions

The strains, plasmids, and primers used in this study are described in Supplementary Tables 4, 5, and 6, respectively. Strain construction details are available in a Supplementary Note. *C. crescentus* wild-type strain NA1000 and its derivatives were grown at 30 °C in peptone-yeast-extract (PYE) medium for routine culturing. To control serine concentration for the serine auxotrophic strain, *C. crescentus* was grown in Hutner-Imidazole-Glucose-Glutamate (HIGG) media[46] with variable amounts of serine (0-10 mM). *E. coli* strains were grown at 37 °C in LB medium. When necessary, antibiotics were added at the following concentrations: kanamycin 30 μg/ml in broth and 50 μg/ml in agar (abbreviated 30:50) for *E. coli* and 5:25 for *C. crescentus*; tetracycline 12:12 *E. coli* and 1:2 *C. crescentus*; spectinomycin 50:50 *E. coli* and 25:100 *C. crescentus*; and ampicillin 50:100 *E. coli*. Gene expression was induced in *C. crescentus* with either 0.3% (w/v) xylose or 0.5 mM vanillate. *Streptomyces aurantiacus* was grown in International Streptomyces Project Synthetic Salts-Starch Medium (ISP4) at 30 °C.

Genetic screen for ceramide synthesis enzymes

A conjugation-competent and diaminopimelic acid (DAP) auxotrophic strain of *E. coli* (MFDpir,[47]) carrying the kanamycin-encoding mini-Tn5 plasmid pBAM1 (Addgene #60487,[48]) was grown overnight in LB media containing 0.3 mM DAP. Wild-type *C.*

crescentus was grown overnight in PYE. In a microcentrifuge tube, 1 ml of *C. crescentus* was mixed with 100 µl of *E. coli*, the cells were washed once in PYE, and the final cell pellet was resuspended in 20 µl PYE. The concentrated cell sample was dropped onto a PYE agar plate containing 0.3 mM DAP and incubated at 30 °C for 6 hr. After incubation, the cells were scraped into 1 ml of PYE, vortexed, and spread onto PYE agar plates containing 25 µg/ml kanamycin and 200 µg/ml polymyxin B. In the absence of DAP, the donor *E. coli* strain could not grow, the kanamycin selected for transposon insertions, and the polymyxin B selected for potentially ceramide-deficient cells. Colonies were picked into duplicate 96-well plates containing 200 µl PYE per well +/− 2 µl bacteriophage ϕCr30. Each plate had one well of wild-type control and one well with no cells, as a control for contamination. Approximately 20 sets of duplicate plates were inoculated. Plates were incubated overnight at 30 °C and growth was measured in a BMG Labtech CLARIOstar plate reader by absorbance at 660 nm. The 94 phage-containing wells that had the lowest OD_{660} were considered potential hits. The corresponding wells from the non-infected plates were consolidated into new 96-well plates and treated +/− phage as above. Growth curves were acquired for 27 hr on a BMG Labtech CLARIOstar plate reader incubating at 30 °C with shaking. The ratio of the final to the maximal OD_{660} for each well was calculated and normalized to the wild-type control. Wells with a ratio less than that of the wild-type control were kept for further characterization. To determine the site of transposon insertion we used arbitrarily-primed PCR with primer pairs EKS153/S159 and EKS154/S160 as previously described[48].

Cloning and purification of *C. crescentus* Spt

The *ccna_01220* gene was amplified with primers EK1107/1108. A C-terminal 6-histidine tag expression vector (pET-28a, EMD Biosciences) was amplified with primers EK1131/1106 and the insert was ligated using HiFi Assembly (New England Biolabs). The resulting plasmid was transformed into *E. coli* BL21 (DE3) cells. One colony was grown overnight in Terrific Broth (TB)/kanamycin at 37 °C with shaking. The inoculant was diluted into TB/kanamycin to OD_{600} of 0.1. When the OD_{600} reached 0.8, protein expression was induced with 0.5 mM isopropyl-β-D-1-thiogalactopyranoside (IPTG), and cultures were grown at 16 °C overnight. Cells were harvested by centrifugation at 5,000 x *g* for 7 min. The cell pellets were resuspended in 20 mM potassium phosphate buffer, pH 7.5, 250 mM NaCl, 30 mM imidazole and 25 µM pyridoxal phosphate (PLP). The cells were sonicated on ice (Soniprep 150, 10 cycles of 30 seconds on/30 seconds off), cell lysates were cleared by centrifugation at 24,000 x *g* for 40 min, and supernatants were filtered through a 0.45 µm filter. The recombinant Spt was purified using an Äkta FPLC system (Cytiva) and a HisTrap HP 1 ml Ni^{2+} column (Cytiva) with an imidazole gradient from 30 mM to 500 mM, followed by size exclusion chromatography (SEC) on a HiLoad 16/600 Superdex 200 preparatory grade column (Cytiva) with a buffer containing 20 mM potassium phosphate, pH 7.5, 250 mM NaCl, 10% (v/v) glycerol and 25 µM PLP. The purification was monitored by SDS-PAGE and Coomassie blue staining.

Cloning and purification of *C. crescentus* bCerS

The *ccna_01212* gene was amplified with primers EK1199/1269 and cloned into the NdeI/HindIII site of plasmid pET-28a to generate an N-terminal 6-histidine tag. The construct was

transformed into *E. coli* BL21 (DE3) competent cells. One colony was grown overnight in LB broth/kanamycin at 37 °C with shaking. The inoculant was diluted into LB/kanamycin to OD_{600} of 0.1. When the OD_{600} reached 0.8, protein expression was induced with 1 mM IPTG, and cultures were grown at 16 °C overnight. Cells were harvested by centrifugation at 5,000 x *g* for 7 min. The cell pellets were resuspended in 50 mM Tris-HCl, pH 8.0, 250 mM NaCl, and 30 mM imidazole. The cells were sonicated on ice (Soniprep 150, 10 cycles of 30 seconds on/30 seconds off), cell lysates were cleared by centrifugation at 24,000 x *g* for 40 min, and supernatants were filtered through a 0.45 μm filter. The recombinant bCerS was purified using an Äkta FPLC system (Cytiva) and a HisTrap HP 1 ml Ni^{2+} column (Cytiva) with an imidazole gradient from 10 mM to 500 mM, followed by size exclusion chromatography (SEC) on a HiLoad 16/600 Superdex 200 preparatory grade column (Cytiva) with a buffer containing 50 mM Tris-HCl, pH 8.0, 250 mM NaCl, and 10% (v/v) glycerol. The purification was monitored by SDS-PAGE and Coomassie blue staining.

Mass Spectrometry of recombinant proteins

Purified Spt and bCerS were analyzed in positive ion mode using a liquid chromatography system connected to a Waters Synapt G2 QTOF with an electrospray ionization (ESI) source. 10 μL of 10 μM protein was injected into a Phenomenex C4 3.6 μm column. The conditions for the qTOF were source temperature 120 °C, backing pressure 2 mbar, and sampling cone voltage 54V. The protein was eluted with a 12-minute gradient, starting at 5% acetonitrile with 0.1% formic acid to 95% acetonitrile. The resulting spectra were analyzed using MassLynx V4.1 software (Waters Corporation)

Determination of kinetic constants for *C. crescentus* Spt

Spt kinetic parameters were determined using a 5,5'-dithiobis-(2-nitrobenzoic acid) (DTNB) assay as previously described[16]. The enzyme kinetic assay was carried out in a 96 well microtiter plate containing 0.4 mM DTNB, 1 μM Spt enzyme, 20 mM L-serine, 1-1000 μM C16:0/1-CoA for K_m-C16:0/1-CoA determination or 0.4 mM DTNB, 1 μM Spt enzyme, 0.1-100 mM L-serine, 250 μM C16:0/1-CoA for K_m-L-Ser determination in a buffer containing 100 mM HEPES, 250 mM NaCl, pH 7.0. The experiments were monitored in a BioTek Synergy HT plate reader at 412 nm in 1 min intervals for 60 minutes at 30 °C. The enzyme kinetic constants were calculated by fitting the Michaelis-Menten equation to a plot of reaction rate versus concentration using Origin 2019 (OriginLab).

Assessing sphingolipid products using MALDI-TOF-MS

Spt reaction products were desalted using OMIX C4 pipette tips (Agilent) and eluted in 100% acetonitrile (ACN) containing 0.2% formic acid. 1 μL of first matrix seed (20 mg/ml alpha-cyano-4-hydroxycinnamic acid (CHCA) in methanol/acetone (2:3, v/v) was spotted onto a MTP 384 ground steel plate (Bruker) and left to air dry. The samples were mixed with the second matrix (20 mg/ml CHCA in 50% ACN within 0.25% trifluoroacetic acid (TFA)) in a 1:1 ratio, and 1 μL of the mixture was spotted on top of the CHCA-acetone layer and left to air-dry. The samples were analyzed in reflector mode using a calibrated Bruker UltrafleXtreme MALDI-TOF-mass spectrometer. The analysis was carried out in positive ion mode. The laser power was adjusted to provide optimum signal. Each sample was tested with 500 laser shots and each spectrum was a sum of over 5000 shots. Spectra were acquired

over a range of *m/z* 200-1500. The data acquisition software used was Flex Control version 3.4. The data was analyzed using Data Analysis version 4.4 software.

Enzymatic activity assay for *C. crescentus* bCerS

The reactions were carried out with 2 μM bCerS, 40 μM 3-ketodihydrosphingosine (3-KDS) (dissolved in 0.1% v/v ethanol) and 50 μM C16-CoA for at least 1 hour in a buffer containing 20 mM HEPES, 25 mM KCl, 2 mM $MgCl_2$, pH 7.5. The reaction products were extracted using the Bligh-Dyer method[47] and characterized by LC/MS as described below. To assay bCerS substrate specificity, the reaction was carried out as above using equimolar amounts of C8-C24-CoA (total acyl-CoA concentration remained 50 μM).

Determination of kinetic constants for *C. crescentus* bCerS

bCerS kinetic parameters were determined using a DTNB assay as previously described above for Spt. The enzyme kinetic assay was carried out in a 96 well microtiter plate containing 1 mM DTNB, 1.2 mg/ml bCerS enzyme, 0 or 40 μM 3-KDS, and 1-500 μM C16:0-CoA for K_m-C16:0-CoA determination in a buffer containing 100 mM HEPES, 150 mM NaCl, pH 7.5. The experiments were monitored in a BioTek Synergy HT plate reader at 412 nm in 30 second intervals for 60 minutes at 30 °C. The enzyme kinetic constants were calculated by fitting the Michaelis-Menten equation to a plot of reaction rate versus concentration using Origin 2019 (OriginLab).

Lipid extraction

C. crescentus strains were grown overnight (5 ml) and lipids were extracted by the method of Bligh and Dyer[49]. Cells were harvested in glass tubes at 10,000 x *g* for 30 min and the supernatant was removed. The cells were resuspended in 1 ml of water, 3.75 volumes of 1:2 (v/v) chloroform: methanol was added, and the samples were mixed by vortexing. Chloroform (1.25 volumes) and water (1.25 volumes) were added sequentially with vortexing to create a two-phase system and the samples were centrifuged at 200 x *g* for 5 minutes at room temperature. The bottom, organic phase was transferred to a clean tube with a Pasteur pipette and washed twice in “authentic” upper phase. Subsequently, the residual organic phase with the lipids was collected and dried under argon.

Lipid analysis by normal phase LC/ESI–MS/MS

Methods for lipid analysis by normal phase LC/ESI–MS/MS have been described[50]. Briefly, normal phase LC was performed on an Agilent 1200 Quaternary LC system equipped with an Ascentis Silica HPLC column, 5 μm, 25 cm × 2.1 mm (Sigma-Aldrich, St. Louis, MO) as described. The LC eluent (with a total flow rate of 300 μl/min) was introduced into the ESI source of a high resolution TripleTOF5600 mass spectrometer (Applied Biosystems, Foster City, CA). Instrumental settings for negative ion ESI and MS/MS analysis of lipid species were as follows: ion spray voltage (IS) = −4500 V; curtain gas (CUR) = 20 psi; ion source gas 1 (GSI) = 20 psi; declustering potential (DP) = −55 V; and focusing potential (FP) = −150 V. The MS/MS analysis used nitrogen as the collision gas. Data analysis was performed using Analyst TF1.5 software (Applied Biosystems, Foster City, CA). A list of the identified lipid species can be found in Supplementary Table 2. A representative total ion

chromatogram (TIC) and its corresponding extracted ion chromatogram (EIC) is available in Extended Data Figs. 3c-d. The peak areas of the EICs of major lipid species are compiled in Supplementary Table 3.

Cell permeabilization and labeling

Chloroform-saturated Tris buffer was prepared by mixing 50 mM Tris, pH 7.4 with chloroform (70:30) and shaking the mixture at room temperature for 30 min. Cells to be permeabilized were collected via centrifugation (2 min at 6,000 x *g*, 4 °C) and resuspended in an equal volume of the aqueous phase of the chloroform-saturated Tris buffer. Resuspended cells were rocked for 45 min at room temperature and then washed twice in 50 mM Tris, pH 7.4 (via centrifugation for 10 min at 5,000 x *g*) to remove residual chloroform. Control cells were treated as above, but incubated in 50 mM Tris, pH 7.4 without chloroform.

Fluorescence microscopy

Cells harboring fluorescent fusions were induced overnight with 0.3% xylose and permeabilized as described above. The permeabilizes cells were spotted onto 1% agarose pads. Fluorescence microscopy was performed on a Nikon Ti-E inverted microscope equipped with a Prior Lumen 220PRO illumination system, CFI Plan Apochromat 100X oil immersion objective (NA 1.45, WD 0.13 mm), Zyla sCMOS 5.5-megapixel camera (Andor), and NIS Elements v, 4.20.01 for image acquisition.

Phylogenetic analysis of bacterial ceramide synthesis genes

Following our identification of Spt, bCerS, and CerR as key enzymes in ceramide synthesis in *C. crescentus*, we used BLASTP to find the closest protein homologues in the known ceramide producers *P. gingivalis*, *M. xanthus*, and *B. stolpii* (see Supplementary Data 1). Using each of these proteins as a query, we used TBLASTN to find related proteins in the NCBI prokaryotic representative genomes database (5,700+ representative bacterial organisms). E-value cutoffs were determined by performing a traditional BLASTP with each protein and getting the approximate E-value cutoff for the top 250 hits (see Supplementary Data 1). TBLASTN settings were chosen to only take the top hit for each organism, and we collected the organism name, taxonomic ID, sequence start and end position, strand orientation, and protein sequence. Following the TBLASTN searches, the data were combined and filtered to remove duplicates. We identified organisms that contained hits for all three target genes. To facilitate comparison of these organisms, we made *in silico* fusions by concatenating the Spt, CerR, and bCerS protein sequences. These fused sequences were aligned using MUSCLE aligner[51]. Phylogenetic trees were prepared using RAxML (Randomized Axelerated Maximum Likelihood version 8.2.12)[52] with 100 bootstraps and a maximum-likelihood search. RAxML was run on the CIPRES Portal at the San Diego Supercomputer Center[53]. Similar phylogenetic analyses were performed for the individual enzymes (see Extended Data Fig. 6). The taxonomic class for each organism was retrieved from the NCBI taxonomy database using the R package taxize[54]. Phylogenetic trees were visualized in R using the packages ggtree[55], ape[56], treeio[57], and ggplot2[58].

Phylogenetic analyses of ceramide synthesis genes

To get a representative set of sequences from across the eukaryotic domain, we used BLASTP on the NCBI server to find the top 500 eukaryotic hits for CerS from humans (CerS1, Accession P27544.1), *Arabidopsis thaliana* (Lag1P, Accession NP_001184985), and *Saccharomyces cerevisiae* (Lag1P, Accession AAA21579.1). The results were cleaned to remove duplicate hits; in order to compare roughly the same number of proteins in each group, 250 hits were chosen at random using the Linux "shuf" command. The same protocol was used for the following Spt and KDSR queries: human (Accessions NP_006406.1 and NP_002026.1), *A. thaliana* (Accessions NP_190447.1 and NP_187257), and *S. cerevisiae* (Accessions CAA56805.1 and P38342). The yeast CerS and KDSR proteins were then used to find the closest homologues in bacteria using BLASTP. Short-chain dehydrogenases similar to yeast KDSR were identified; by contrast, yeast CerS had a single partial match (45% query coverage, E-value=4.0) in *Orenia metallireducens*. *C. crescentus* CerR was used as a query to find the closest eukaryotic homologues, which identified NDUF9A proteins. A reverse-BLAST identified CCNA_03718 as the closest *C. crescentus* NDUF9A homologue, which was then used to identify other bacterial NDUF9A homologues. To trace the lineage of bCerS, we used the following protein queries to identify eukaryotic Gcn5 proteins: human (Accession AAC39769.1) and *S. cerevisiae* (Accession NP_011768.1). We identified bacterial GNAT proteins using *C. crescentus* bCerS as a BLASTP query to search the entire NCBI bacterial database. The eukaryotic Spt proteins were compared to the bacterial Spt proteins identified in Supplemental Data 1. Phylogenetic trees for the Spt, CerR/KDSR/NDUF9A, and CerS/Gcn5/GNAT/bCerS proteins were prepared with MUSCLE and RAxML and visualized with R as described above.

Extended Data

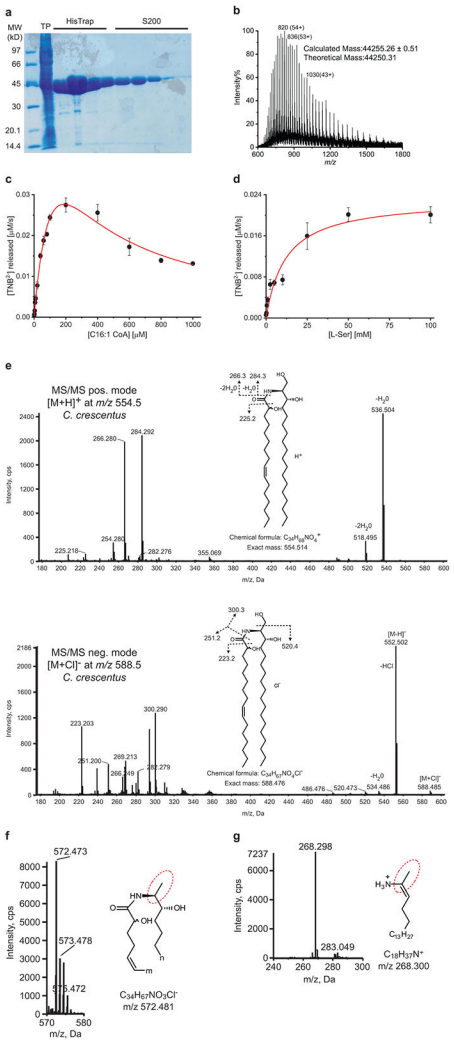

Extended Data Fig. 1. C. crescentus Spt can use a variety of substrates.

(a) Recombinant CCNA_01220 (Spt) was purified as described in the methods. TP is total protein extract. Recombinant protein was independently purified at least three times with similar purities as judged by Coomassie staining. (b) The identity of the purified Spt protein was confirmed by LC/ESI/MS. The peaks correspond to the relative abundances of the multiple-charged species of the protein analyte; the charge is indicated in parenthesis. (c-d) Kinetic analyses of CCNA_01220 determined the Km values for C16:1-CoA (0.045 ± 0.004 mM. Panel c) and L-serine (11.97 ± 2.18 mM. Panel d) (n=3; data are presented as mean +/− SD). (e) Positive- and negative-ion mode MS/MS analysis of ceramides from wild-type C. crescentus (see Fig. 2a) confirm that the desaturation and additional hydroxyl group are located on the acyl chain moiety. (f-g) Serine auxotrophic ΔserA cells were grown in HIGG media without serine, and lipids were isolated for MS/MS analysis. (f) Negative ion ESI/MS shows the [M + Cl]− ion of 1-deoxyceramide emerging at 2 to 3 min. The incorporation of alanine rather than serine is designated with a red-dashed oval. (g) MS/MS analysis of the parent ion confirmed the identity of the 1-deoxyceramide.

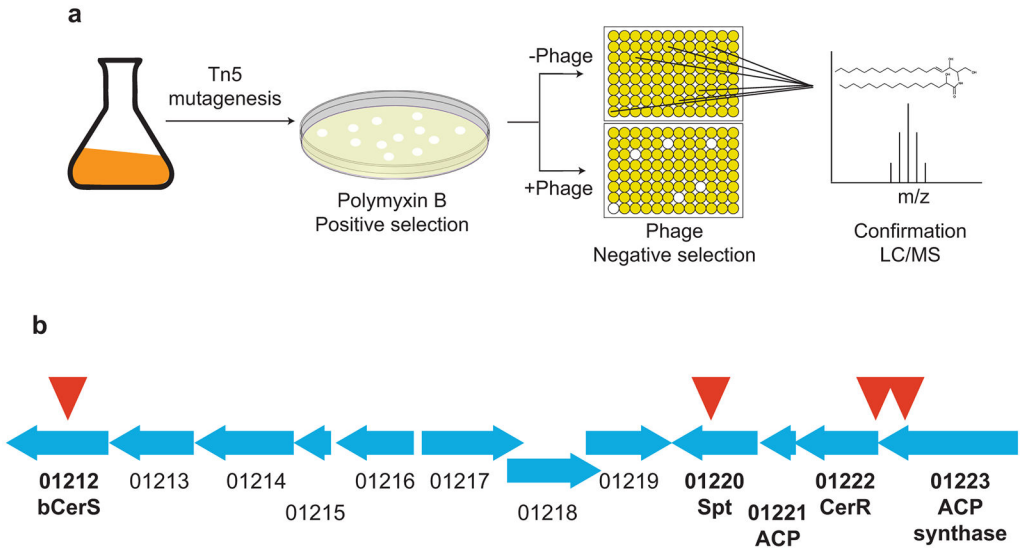

Extended Data Fig. 2. A transposon screen for ceramide-deficient mutants yielded multiples hits in the Spt genomic locus.

(a) The schematic illustrates the tandem positive/negative selection screen used to identify ceramide synthesis genes. Transposon mutants were initially screened for growth on polymyxin B. Resistant clones were then assayed for increased sensitivity to bacteriophage ϕCr30. The effects on ceramide production were assessed by LC/MS. (b) The sites of transposon insertions are indicated with a red triangle. Gene annotations are based on the results presented in Figures 1-3 and Extended Data Figures 3-5. The exact coordinates of the insertions are provided in Supplementary Table 1.

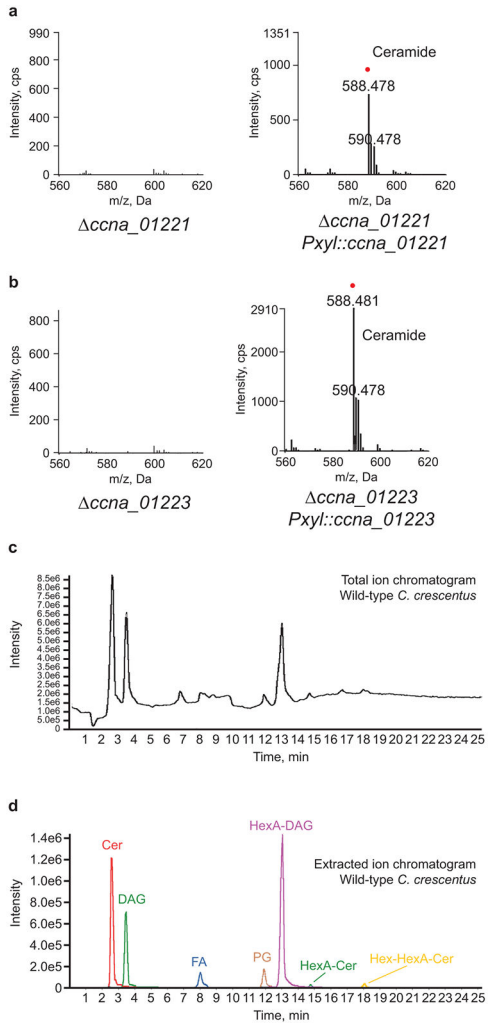

Extended Data Fig. 3. Acyl carrier protein and ACP-synthetase are required for ceramide synthesis in C. crescentus.

(a-b) ACP (ccna_01221) and ACP-synthetase (ccna_01223) deletion strains and the corresponding complementation strains were grown overnight in PYE with 0.3% (w/v) xylose. Negative ion ESI/MS shows the [M + Cl]− ions of the lipids emerging at 2 to 3 min. Ceramide species are labelled with a red dot. (c) A total ion chromatogram (TIC) and (d) the corresponding extracted ion chromatogram (EIC) of lipids from C. crescentus grown in PYE media show the major species present in the lipid extract.

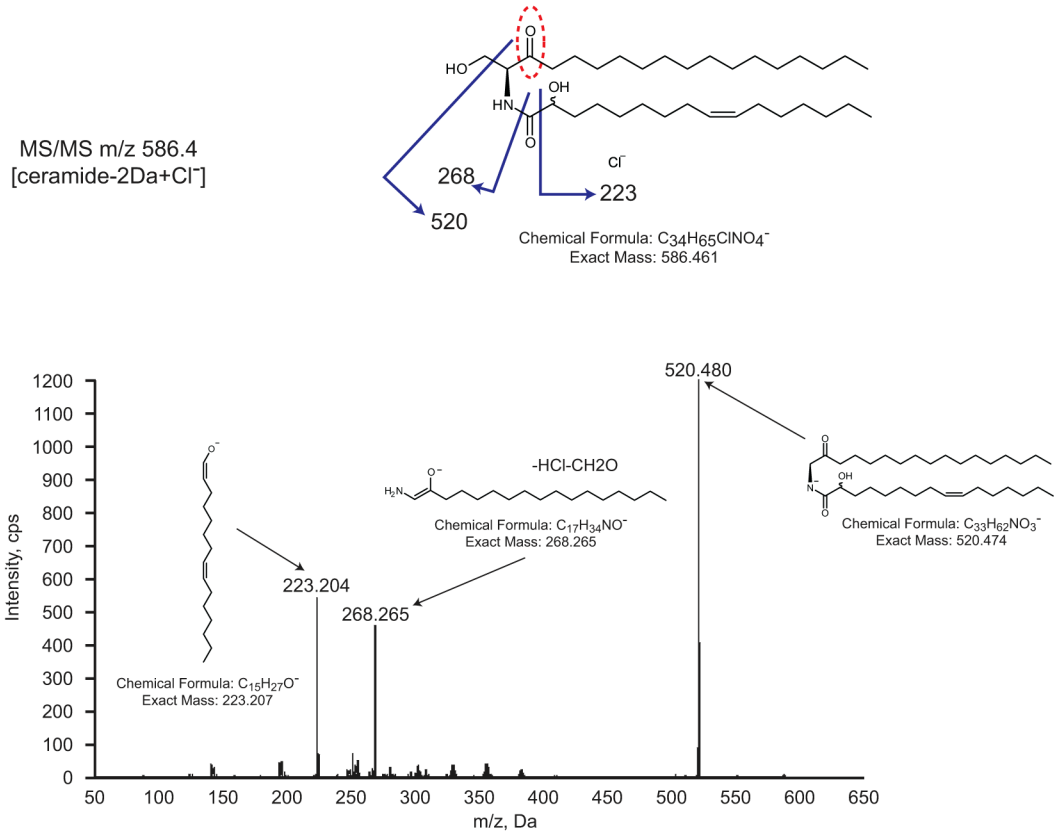

Extended Data Fig. 4. MS/MS confirms the production of oxidized ceramide in the absence of CerR.

The oxCer lipid produced in the ΔcerR strain (Fig. 2a, middle panel) was subjected to MS/MS analysis. The fragment ions confirm the presence of two oxidized C═O bonds.

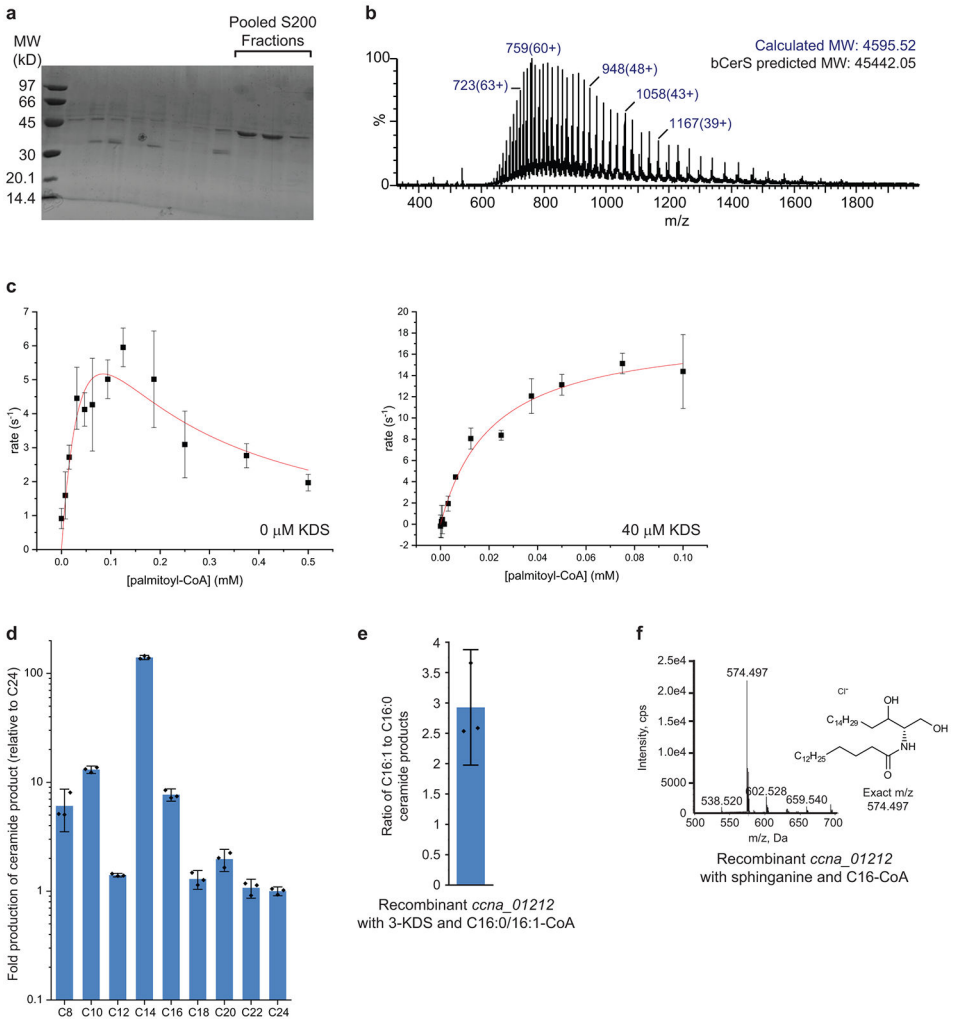

Extended Data Fig. 5. Purification of C. crescentus bCerS.

(a) bCerS was purified as described in the Materials and Methods. SDS-PAGE analysis confirmed protein purity following S200 size-exclusion chromatography. The indicated fractions were pooled for MS characterization. Recombinant protein was independently purified at least three times with similar purities as judged by Coomassie staining. (b) The identity of the purified bCerS protein was confirmed by LC/ESI/MS. The ions for two species were detected, which differed by 178 Da (top); this difference is due to spontaneous alpha-N-6-phosphogluconoylation which is commonly observed in His-tagged proteins expressed in E. coli41. The protein molecular weight was calculated using the relative abundances of the multiple-charged species of the protein analyte (bottom); the charges are indicated in parenthesis. (c) Kinetic analyses of CCNA_01212 in the absence (left) and presence (right) of 3-KDS determined the Km,app value for C16:0-CoA (21.3 ± 4.1 μM) (n=3, data are presented as mean +/− SD). (d) To determine the substrate specificity of C. crescentus bCerS, we incubated the recombinant enzyme with 40 μM 3-KDS and an equimolar mixture of fatty acid-CoA (C8-C24) with a total final concentration of 50 μM. The reaction proceeded for 1 hr and the reaction products were analyzed by ESI/MS. The integrated ion counts were normalized to C24 (n=3, data are presented as mean +/− SD).

(e) To determine the acyl-chain saturation preference of C. crescentus bCerS, we incubated the recombinant enzyme with 40 μM 3-KDS and an equimolar mixture of C16:0-CoA and C16:1-CoA, with a total final concentration of 50 μM. The reaction proceeded for 1 hr and the reaction products were analyzed by NPLC-ESI/MS in the negative ion mode to determine the ratio of ceramide products produced (C16:0 product, [M+Cl]− at m/z 572.481; C16:1 product, [M+Cl]− at m/z 570.466) (n=3, data are presented as mean +/− SD). (f) Recombinant bCerS was incubated with 40 μM sphinganine and 50 μM C16:0-CoA for 1 hr and the reaction product was analyzed by ESI/MS.

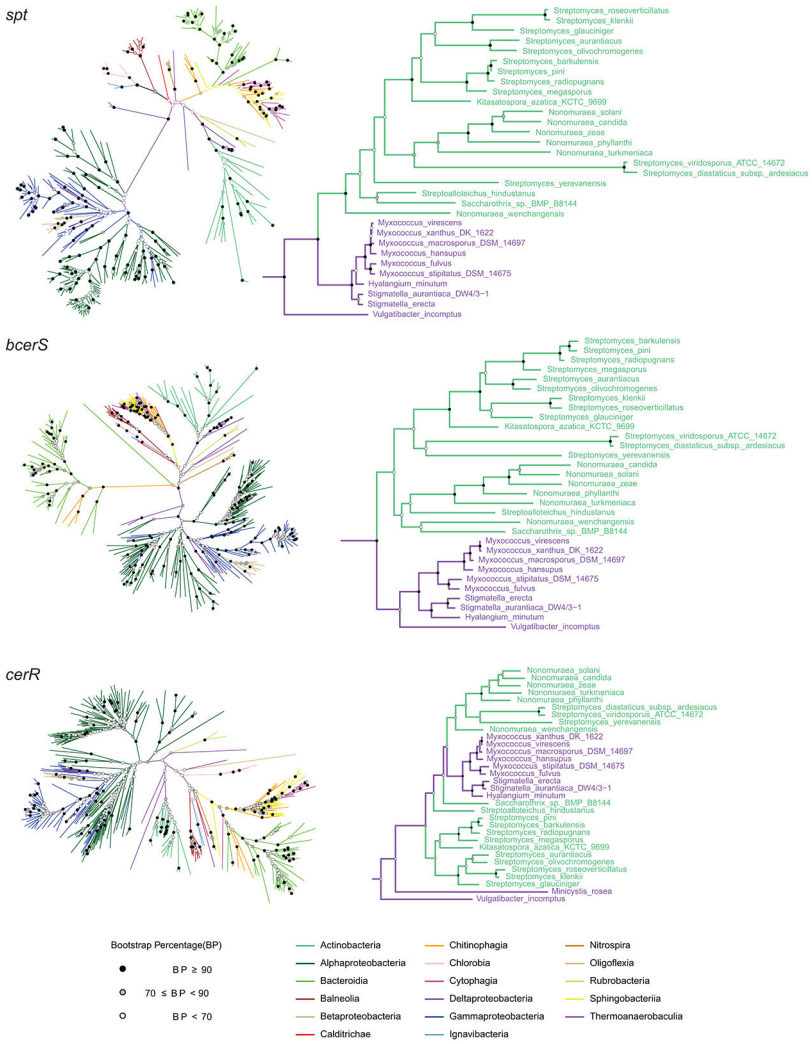

Extended Data Fig. 6. Phylogeny of bacterial ceramide synthesis enzymes.

Unrooted phylogenetic trees were created for the individual Spt, CerR, and bCerS proteins from the organisms identified in Fig. 3d (left). A zoomed in view of the branches of the trees containing Actinobacteria show the close relationship between these Gram-positive organisms and Deltaproteobacteria (right). For each of the individual enzymes, the closest homologues for the Actinobacteria are found in Deltaproteobacteria. Bootstrap percentages are indicated by the filled circles at each node.

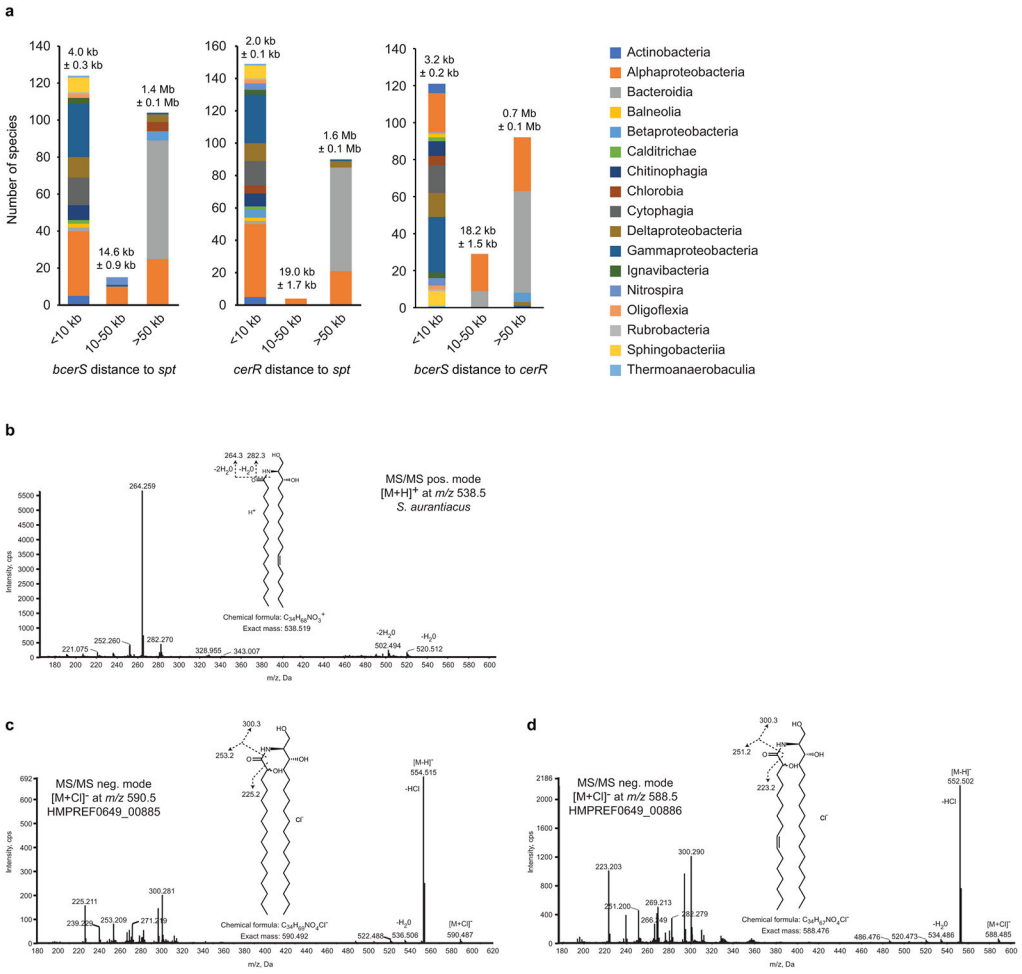

Extended Data Fig. 7. Ceramide synthesis orthologues.

(a) Using the genomic coordinates acquired during the phylogenetic analysis of bacterial ceramide genes, the distances between spt, bcerS, and cerR were calculated. The histogram columns are colored by taxonomic class. The numbers above the columns are the average distance ± the standard error of the mean. (b) MS/MS analysis of ceramides from S. aurantiacus confirm that the desaturation occurs on the long-chain base. (c) MS/MS analysis of ceramides produced by bCerS homologues from P. buccae (see Fig. 3f) show that HMPREF0649_00885 preferred fully saturated substrates, while HMPREF0649_00886 used a desaturated palmitoyl-CoA substrate.

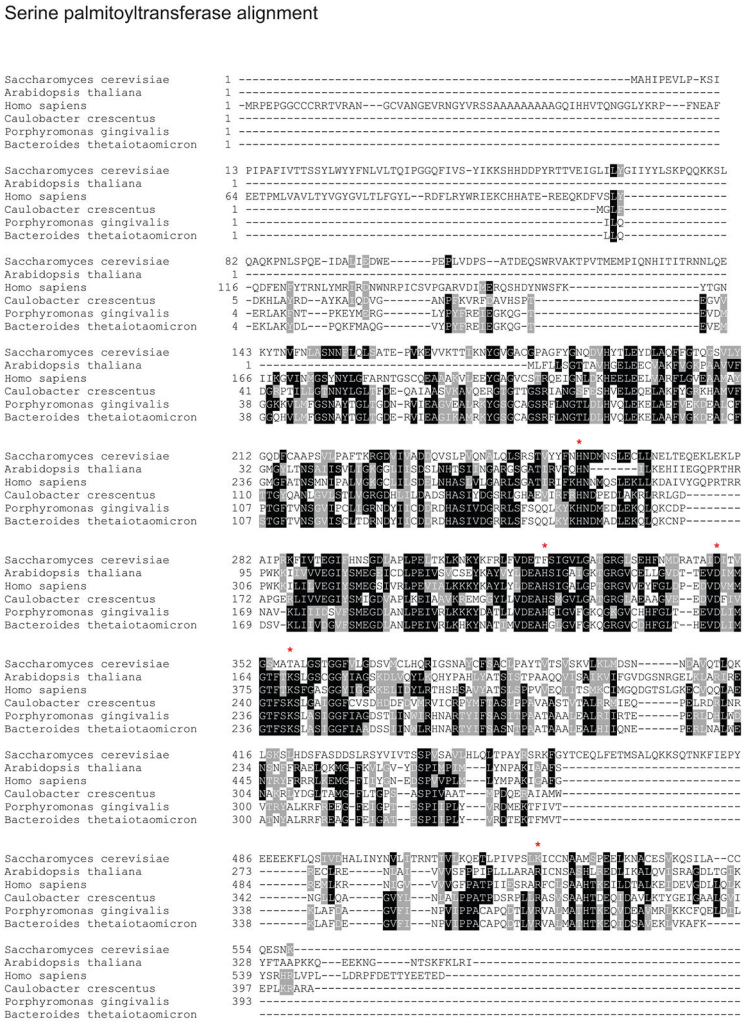

Extended Data Fig. 8. Alignment of Spt across taxonomic domains suggests a common evolutionary ancestor.

Protein alignment of several eukaryotic and bacterial Spt enzymes was performed using Clustal Omega[44]. Previously characterized active site residues are indicated by (*)[45].

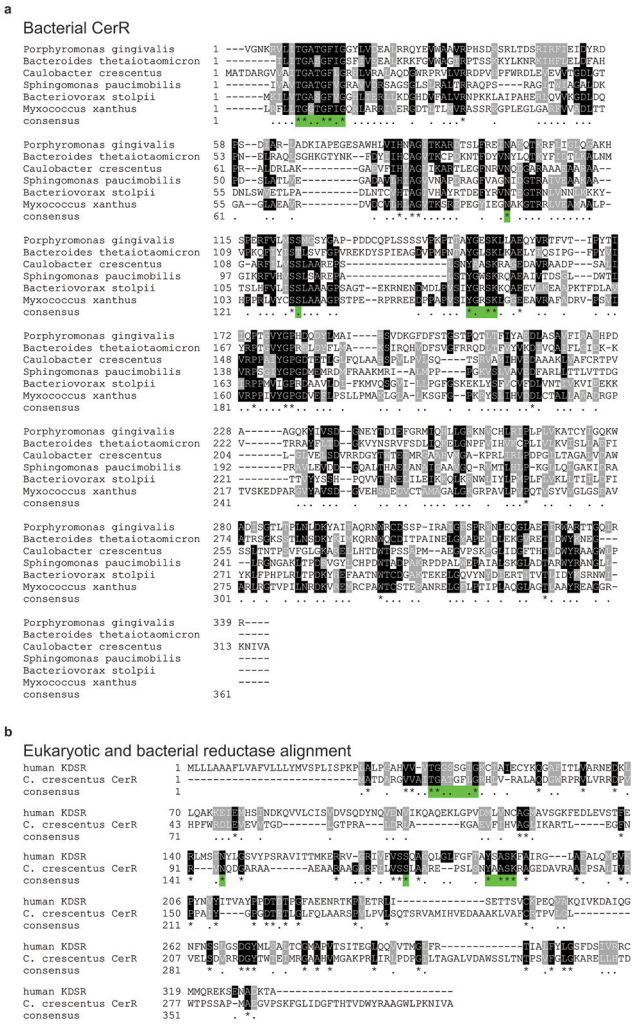

Extended Data Fig. 9. Alignment of reductase enzymes suggests independent evolution of CerR and KDSR.

(a-b) Alignments of bacterial CerR proteins (a) or C. crescentus CerR and human KDSR (b) were done using Clustal Omega[44]. Green-highlighted residues are active site amino acids in KDSR[34]. The YxxxK motif is the reductase active site and the TGxxxGxG motif is the NAD binding site. Note that the bacterial NAD binding site, TGxxGFxG, is different from the eukaryotic site.

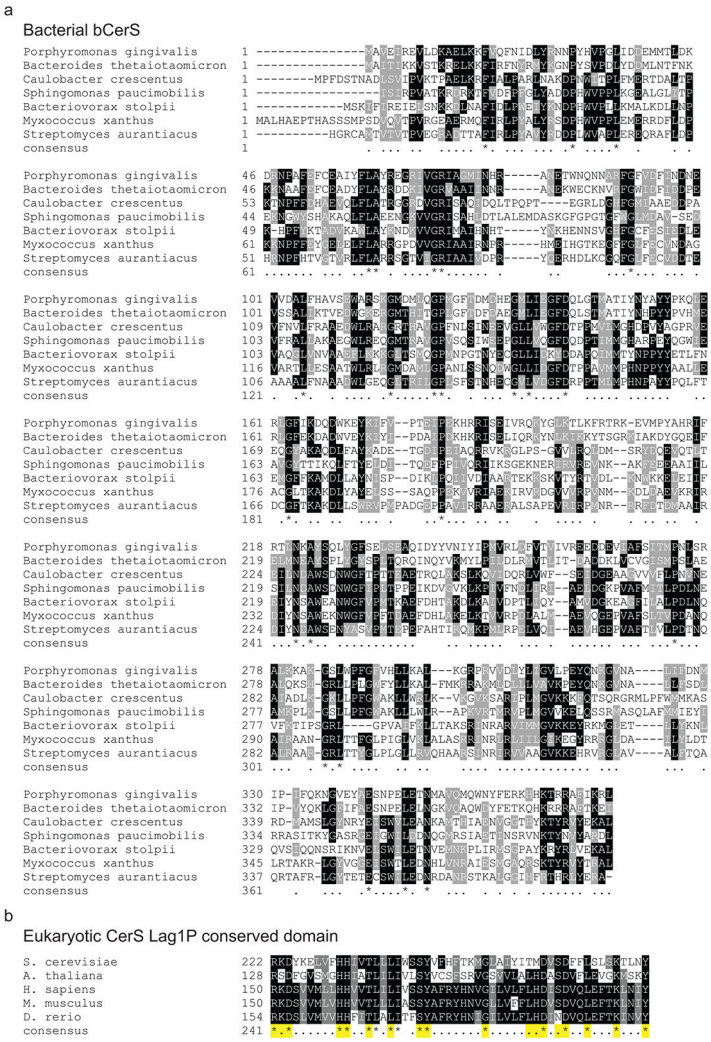

Extended Data Fig. 10. Alignment of ceramide synthase enzymes suggests independent evolution of bCerS and CerS.

(a) bCerS homologues were aligned using Clustal Omega[44]. (b) The conserved Lag1P domains from eukaryotic CerS proteins[35,36] were aligned with Clustal Omega[44]. Active-site residues are highlighted in yellow. The Lag1P domain is absent from bCerS.

Supplementary Material

Refer to Web version on PubMed Central for supplementary material.

Acknowledgments:

The authors thank Carla Cugini (Rutgers University) for providing *P. gingivalis* genomic DNA for cloning. The authors also thank Anthony Geneva (Rutgers University-Camden) for helpful discussions. Funding was provided by National Science Foundation grants MCB-1553004 and MCB-2031948 (E.A.K.), National Institutes of Health grants GM069338 and R01AI148366 (Z.G.), and Biotechnology and Biological Sciences Research Council grants BB/M010996/1 and BB/T016841/1 (D.J.C.).

Data availability:

The raw data for Figure 1C and Extended Data Figures 1c-d, 5c-e, and 7a are provided as Microsoft Excel files in the supplementary information (Source Data 1-4). The data for the bioinformatic analyses was obtained from the following publicly available NCBI resources: NCBI Prokaryotic Representative Genomes: https://ftp.ncbi.nlm.nih.gov/genomes/GENOME_REPORTS/prok_representative_genomes.txt. Accession numbers for the proteins used for BLAST analyses are as follows. Bacterial Spt homologues: *C. crescentus* YP_002516593.1; *P. gingivalis* BAG34240; *M. xanthus* ABF87747; *B. stolpii* BAF73753. Bacterial bCerS homologues: *C. crescentus* YP_002516585.1; *P. gingivalis* BAG32893; *M. xanthus* ABF92629; *B. stolpii* WP_102243213. Bacterial CerR homologues: *C. crescentus* YP_002516595.1; *P. gingivalis* BAG34405; *M. xanthus* ABF87537; *B. stolpii* WP_102243212. Eukaryotic CerS homologues: Human P27544.1; *A. thaliana* NP_001184985; *S. cerevisiae* AAA21579.1. Eukaryotic Spt homologues: Human NP_006406.1; *A. thaliana* NP_190447.1; *S. cerevisiae* CAA56805.1. Eukaryotic KDSR homologues: Human NP_002026.1; *A. thaliana* NP_187257; *S. cerevisiae* P38342. Eukaryotic Gcn5 homologues: Human AAC39769.1 and *S. cerevisiae* NP_011768.1.

References

1. Harrison PJ, Dunn TM & Campopiano DJ Sphingolipid biosynthesis in man and microbes. Nat Prod Rep 35, 921–954 (2018). [PubMed: 29863195]
2. Brown EM et al. Bacteroides-derived sphingolipids are critical for maintaining intestinal homeostasis and symbiosis. Cell Host Microbe 25, 668–680 e667 (2019). [PubMed: 31071294]
3. Moye ZD, Valiuskyte K, Dewhirst FE, Nichols FC & Davey ME Synthesis of sphingolipids impacts survival of Porphyromonas gingivalis and the presentation of surface polysaccharides. Front Microbiol 7, 1919 (2016). [PubMed: 27965646]
4. Stankeviciute G, Guan Z, Goldfine H & Klein EA Caulobacter crescentus adapts to phosphate starvation by synthesizing anionic glycoglycerolipids and a novel glycosphingolipid. mBio 10, e00107–00119 (2019). [PubMed: 30940701]
5. Ahrendt T, Wolff H & Bode HB Neutral and phospholipids of the *Myxococcus xanthus* lipodome during fruiting body formation and germination. Appl Environ Microbiol 81, 6538–6547 (2015). [PubMed: 26162876]
6. Kaneshiro ES, Hunt SM & Watanabe Y Bacteriovorax stolpii proliferation and predation without sphingophosphonolipids. Biochem Biophys Res Commun 367, 21–25 (2008). [PubMed: 18086555]
7. Hannun YA & Obeid LM Sphingolipids and their metabolism in physiology and disease. Nat Rev Mol Cell Biol 19, 175–191 (2018). [PubMed: 29165427]
8. Merrill AH Jr. Sphingolipid and glycosphingolipid metabolic pathways in the era of sphingolipidomics. Chem Rev 111, 6387–6422 (2011). [PubMed: 21942574]
9. Ikushiro H, Hayashi H & Kagamiyama H A water-soluble homodimeric serine palmitoyltransferase from Sphingomonas paucimobilis EY2395T strain. Purification, characterization, cloning, and overproduction. J Biol Chem 276, 18249–18256 (2001). [PubMed: 11279212]
10. Yard BA et al. The structure of serine palmitoyltransferase; gateway to sphingolipid biosynthesis. J Mol Biol 370, 870–886 (2007). [PubMed: 17559874]
11. Geiger O, Gonzalez-Silva N, Lopez-Lara IM & Sohlenkamp C Amino acid-containing membrane lipids in bacteria. Prog Lipid Res 49, 46–60 (2010). [PubMed: 19703488]
12. Olea-Ozuna RJ et al. Five structural genes required for ceramide synthesis in *Caulobacter* and for bacterial survival. Environ Microbiol (2020).
13. Wadsworth JM et al. The chemical basis of serine palmitoyltransferase inhibition by myriocin. J Am Chem Soc 135, 14276–14285 (2013). [PubMed: 23957439]

14. Harrison PJ et al. Use of isotopically labeled substrates reveals kinetic differences between human and bacterial serine palmitoyltransferase. J Lipid Res 60, 953–962 (2019). [PubMed: 30792183]
15. Li S, Xie T, Liu P, Wang L & Gong X Structural insights into the assembly and substrate selectivity of human SPT-ORMDL3 complex. Nat Struct Mol Biol 28, 249–257 (2021). [PubMed: 33558762]
16. Raman MC et al. The external aldimine form of serine palmitoyltransferase: structural, kinetic, and spectroscopic analysis of the wild-type enzyme and HSAN1 mutant mimics. J Biol Chem 284, 17328–17339 (2009). [PubMed: 19376777]
17. Raman MC, Johnson KA, Clarke DJ, Naismith JH & Campopiano DJ The serine palmitoyltransferase from Sphingomonas wittichii RW1: An interesting link to an unusual acyl carrier protein. Biopolymers 93, 811–822 (2010). [PubMed: 20578000]
18. Ren J et al. Quantification of 3-ketodihydrosphingosine using HPLC-ESI-MS/MS to study SPT activity in yeast Saccharomyces cerevisiae. J Lipid Res 59, 162–170 (2018). [PubMed: 29092960]
19. Zheng W et al. Ceramides and other bioactive sphingolipid backbones in health and disease: lipidomic analysis, metabolism and roles in membrane structure, dynamics, signaling and autophagy. Biochim Biophys Acta 1758, 1864–1884 (2006). [PubMed: 17052686]
20. Tidhar R et al. Eleven residues determine the acyl chain specificity of ceramide synthases. J Biol Chem 293, 9912–9921 (2018). [PubMed: 29632068]
21. Chow TC & Schmidt JM Fatty acid composition of *Caulobacter crescentus*. Microbiology 83, 369–373 (1974).
22. Okino N et al. The reverse activity of human acid ceramidase. J Biol Chem 278, 29948–29953 (2003). [PubMed: 12764132]
23. Chen M, Markham JE, Dietrich CR, Jaworski JG & Cahoon EB Sphingolipid long-chain base hydroxylation is important for growth and regulation of sphingolipid content and composition in Arabidopsis. Plant Cell 20, 1862–1878 (2008). [PubMed: 18612100]
24. Omae F et al. DES2 protein is responsible for phytoceramide biosynthesis in the mouse small intestine. Biochem J 379, 687–695 (2004). [PubMed: 14731113]
25. Price MN et al. Mutant phenotypes for thousands of bacterial genes of unknown function. Nature 557, 503–509 (2018). [PubMed: 29769716]
26. Kawahara K, Moll H, Knirel YA, Seydel U & Zähringer U Structural analysis of two glycosphingolipids from the lipopolysaccharide-lacking bacterium *Sphingomonas capsulata*. European Journal of Biochemistry 267, 1837–1846 (2000). [PubMed: 10712617]
27. Feng Y & Cronan JE *Escherichia coli* unsaturated fatty acid synthesis: complex transcription of the *fabA* gene and in vivo identification of the essential reaction catalyzed by FabB. J Biol Chem 284, 29526–29535 (2009). [PubMed: 19679654]
28. Christen B et al. The essential genome of a bacterium. Mol Syst Biol 7, 1–7 (2011).
29. Stankeviciute G et al. Differential modes of crosslinking establish spatially distinct regions of peptidoglycan in *Caulobacter crescentus*. Mol Microbiol 111, 995–1008 (2019). [PubMed: 30614079]
30. Rocha FG et al. *Porphyromonas gingivalis* sphingolipid synthesis limits the host inflammatory response. J Dent Res 99, 568–576 (2020). [PubMed: 32105543]
31. Mun J et al. Structural confirmation of the dihydrosphinganine and fatty acid constituents of the dental pathogen *Porphyromonas gingivalis*. Org Biomol Chem 5, 3826–3833 (2007). [PubMed: 18004463]
32. Nguyen M & Vedantam G Mobile genetic elements in the genus Bacteroides, and their mechanism(s) of dissemination. Mob Genet Elements 1, 187–196 (2011). [PubMed: 22479685]
33. Kavanagh KL, Jornvall H, Persson B & Oppermann U Medium- and short-chain dehydrogenase/ reductase gene and protein families : the SDR superfamily: functional and structural diversity within a family of metabolic and regulatory enzymes. Cell Mol Life Sci 65, 3895–3906 (2008). [PubMed: 19011750]
34. Boyden LM et al. Mutations in KDSR cause Recessive Progressive Symmetric Erythrokeratoderma. Am J Hum Genet 100, 978–984 (2017). [PubMed: 28575652]
35. Kageyama-Yahara N & Riezman H Transmembrane topology of ceramide synthase in yeast. Biochem J 398, 585–593 (2006). [PubMed: 16756512]

36. Spassieva S et al. Necessary role for the Lag1p motif in (dihydro)ceramide synthase activity. J Biol Chem 281, 33931–33938 (2006). [PubMed: 16951403]
37. Liebisch G et al. Update on LIPID MAPS classification, nomenclature and shorthand notation for MS-derived lipid structures. J Lipid Res (2020).
38. Yao L et al. A selective gut bacterial bile salt hydrolase alters host metabolism. Elife 7 (2018).
39. Lee MT, Le HH & Johnson EL Dietary sphinganine is selectively assimilated by members of the mammalian gut microbiome. J Lipid Res 62, 100034 (2021). [PubMed: 32646940]
40. Tudzynski B Gibberellin biosynthesis in fungi: genes, enzymes, evolution, and impact on biotechnology. Appl Microbiol Biotechnol 66, 597–611 (2005). [PubMed: 15578178]
41. Huang R, O'Donnell AJ, Barboline JJ & Barkman TJ Convergent evolution of caffeine in plants by co-option of exapted ancestral enzymes. Proc Natl Acad Sci U S A 113, 10613–10618 (2016). [PubMed: 27638206]
42. Dick R et al. Comparative analysis of benzoxazinoid biosynthesis in monocots and dicots: independent recruitment of stabilization and activation functions. Plant Cell 24, 915–928 (2012). [PubMed: 22415274]
43. Kawasaki S et al. The cell envelope structure of the lipopolysaccharide-lacking gram-negative bacterium Sphingomonas paucimobilis. J Bacteriol 176, 284–290 (1994). [PubMed: 8288520]
44. Madeira F et al. The EMBL-EBI search and sequence analysis tools APIs in 2019. Nucleic Acids Res (2019).
45. Lowther J et al. Role of a conserved arginine residue during catalysis in serine palmitoyltransferase. FEBS Lett 585, 1729–1734 (2011). [PubMed: 21514297]

Methods references

46. Poindexter JS Selection for nonbuoyant morphological mutants of *Caulobacter crescentus*. J Bacteriol 135, 1141–1145 (1978). [PubMed: 690072]
47. Ferrieres L et al. Silent mischief: bacteriophage Mu insertions contaminate products of Escherichia coli random mutagenesis performed using suicidal transposon delivery plasmids mobilized by broad-host-range RP4 conjugative machinery. J Bacteriol 192, 6418–6427 (2010). [PubMed: 20935093]
48. Martinez-Garcia E, Calles B, Arevalo-Rodriguez M & de Lorenzo V pBAM1: an all-synthetic genetic tool for analysis and construction of complex bacterial phenotypes. BMC Microbiol 11, 38 (2011). [PubMed: 21342504]
49. Bligh EG & Dyer WJ A rapid method of total lipid extraction and purification. Can J Biochem Physiol 37, 911–917 (1959). [PubMed: 13671378]
50. Guan Z, Katzianer D, Zhu J & Goldfine H *Clostridium difficile* contains plasmalogen species of phospholipids and glycolipids. Biochim Biophys Acta 1842, 1353–1359 (2014). [PubMed: 24983203]
51. Edgar RC MUSCLE: a multiple sequence alignment method with reduced time and space complexity. BMC Bioinformatics 5, 113 (2004). [PubMed: 15318951]
52. Stamatakis A RAxML version 8: a tool for phylogenetic analysis and post-analysis of large phylogenies. Bioinformatics 30, 1312–1313 (2014). [PubMed: 24451623]
53. Miller MA, Pfeiffer W & Schwartz T Creating the CIPRES Science Gateway for inference of large phylogenetic trees. 2010 Gateway Computing Environments Workshop (GCE), 1–8 (2010).
54. Chamberlain SA & Szocs E taxize: taxonomic search and retrieval in R. F1000Res 2, 191 (2013). [PubMed: 24555091]
55. Yu G Using ggtree to visualize data on tree-like structures. Curr Protoc Bioinformatics 69, e96 (2020). [PubMed: 32162851]
56. Paradis E & Schliep K ape 5.0: an environment for modern phylogenetics and evolutionary analyses in R. Bioinformatics 35, 526–528 (2019). [PubMed: 30016406]
57. Wang LG et al. Treeio: An R Package for phylogenetic tree input and output with richly annotated and associated data. Mol Biol Evol 37, 599–603 (2020). [PubMed: 31633786]
58. Wickham H ggplot2: Elegant Graphics for Data Analysis. (Springer-Verlag New York, 2016).

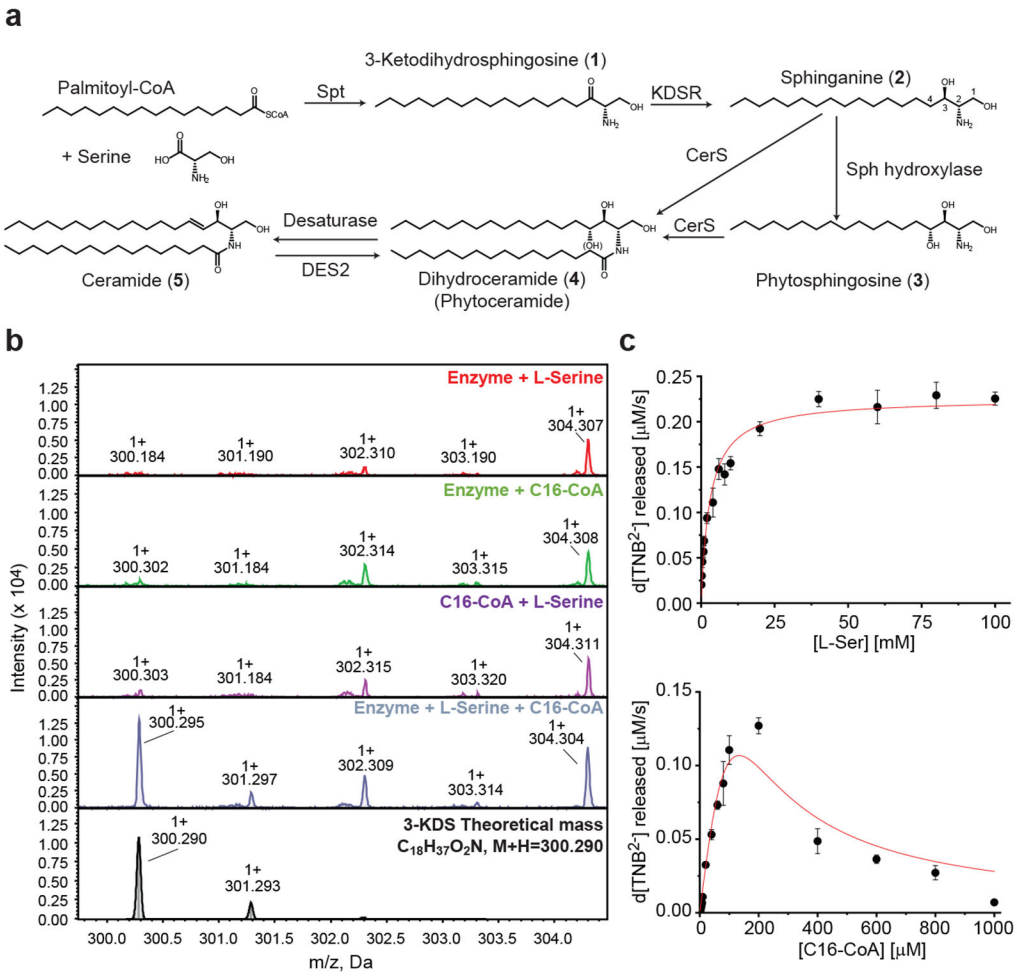

Figure 1. CCNA_01220 is a functional serine palmitoyltransferase (Spt).

(a) The schematic depicts the eukaryotic ceramide synthesis pathway. In some organisms, phytoceramides (**6**) are produced by adding a hydroxyl group (OH) to the sphingoid base (**3**) (Sph) or to ceramide (**5**) (DES2). (b) Recombinant Spt was incubated with the indicated substrates for 1 hr and reaction products were analyzed by MALDI-MS. The final panel shows a theoretical mass spectrum for the expected product, 3-KDS. (c) Kinetic analyses of Spt determined the Km for L-serine (upper) and C16:0-CoA (lower) (n=3; data are presented as mean +/− SD).

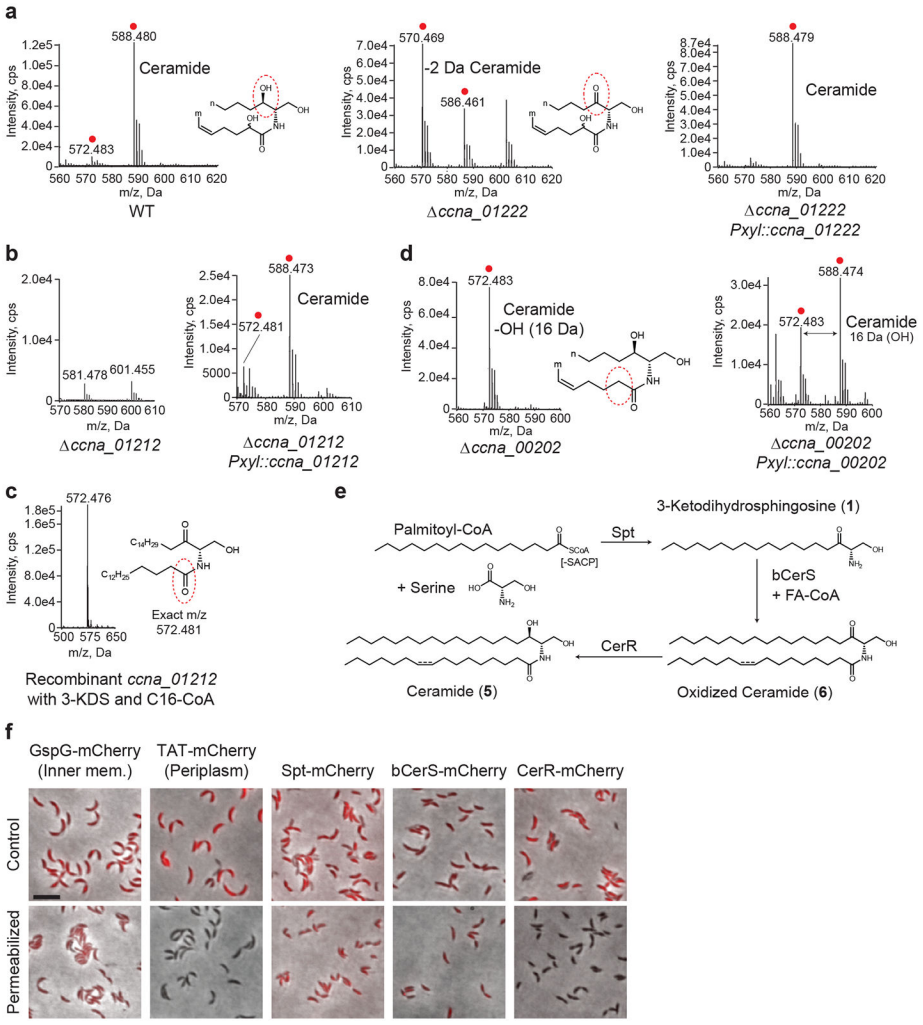

Figure 2. A genetic screen identified ceramide synthesis enzymes.

(a-d) Negative ion ESI/MS shows the $[M + Cl]^-$ ions of the lipids emerging at 2 to 3 min. Ceramide species are labelled with a red dot and the modified lipid moiety is designated with a red-dashed oval. Note that MS/MS analysis of ceramide from *C. crescentus* shows that the desaturation occurs on the acyl chain (see Extended Data Fig. 1e); however, we have not determined the precise position of the double bond. In this, and all subsequent figures, the structural cartoons only indicate which acyl chain is desaturated, but not the exact position of the double bond. Relative quantification of all the major lipid species for each mass spectrum is available in Supplementary Table 3. (a) Lipids were extracted from wild-type, Δ*ccna_01222*, and *ccna_01222*-complemented cells. (b) Lipids were extracted from Δ*ccna_01212* and *ccna_01212*-complemented cells. (c) Recombinant CCNA_01212 was incubated with 40 μM 3-KDS and 50 μM C16:0-CoA for 1 hr and the reaction product was analyzed by normal phase LC/ESI-MS in negative ion mode. (d) Lipids were extracted from Δ*ccna_00202* and *ccna_00202*-complemented cells. (e) Based on the MS data above, we propose the following model for bacterial ceramide synthesis. The genes comprising this synthetic pathway are in close proximity in the genome (see Extended Data Fig. 2b). (f) Cells expressing the indicated fluorescently-tagged proteins were grown overnight in

the presence of inducer. GspG-mCherry and TAT-mCherry are control inner-membrane and periplasmic proteins, respectively. Control and permeabilized cells were imaged by fluorescence microscopy to monitor the loss of fluorescence upon permeabilization. The results are the overlay of phase and fluorescent images. Scale bar = 5 μm.

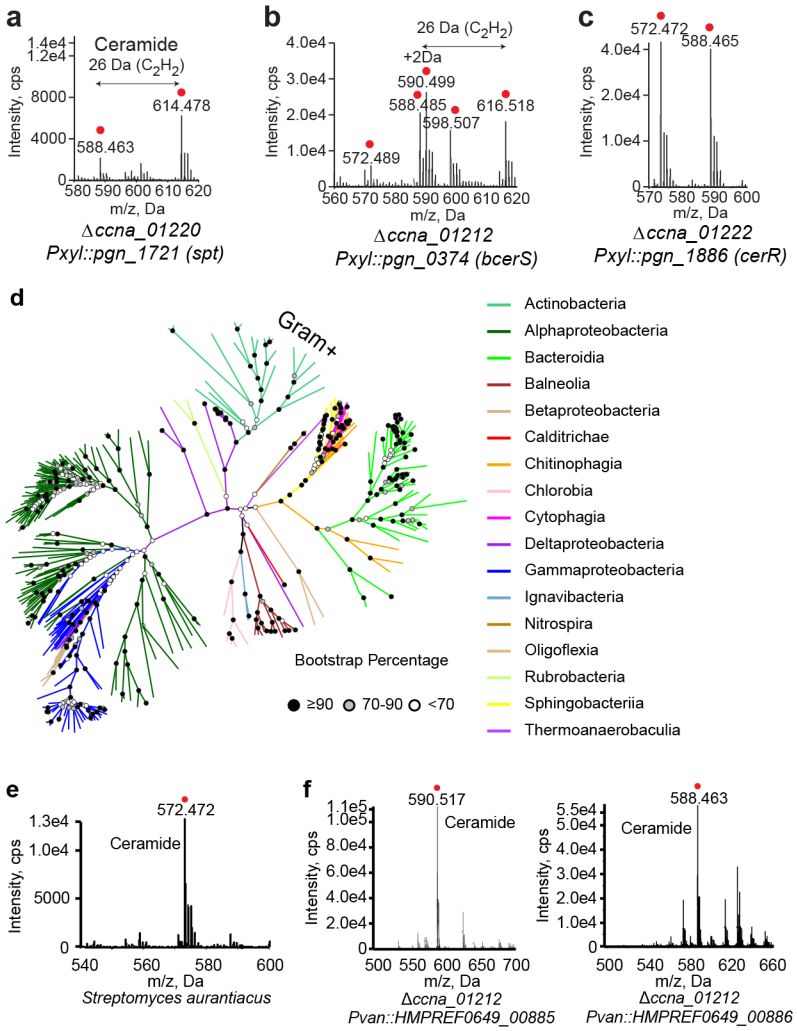

Figure 3. Bioinformatic analysis identifies a wide range of potential ceramide-producing bacteria.

(a-c) Deletions of the *spt* (a), *bcerS* (b), and *cerR* (c) genes in *C. crescentus* were complemented with the indicated homologues from *P. gingivalis*. Lipids extracted from these strains were analyzed by normal phase LC/ESI-MS in negative ion mode. $[M + Cl]^-$ ions of the ceramide species emerging at 2 to 3 min are shown with ceramide species labelled with a red dot. (d) Bacterial species with homologues to all three ceramide synthesis enzymes are clustered by the overall homology of the 3 proteins (see Methods). Bootstrap percentage values are indicated by shaded circles at each node. Branches are colored by taxonomic class and Gram-positive Actinobacteria are labeled. (e) Negative ion ESI/MS shows the $[M + Cl]^-$ ions of the ceramide species (emerging at 2 to 3 min) extracted from *S. aurantiacus*. Ceramide is labelled with a red dot. Determination of the ceramide structure by MS/MS is provided in Extended Data Fig. 7b. (f) Deletion of *bcerS* in *C. crescentus* was complemented by two *bcerS* orthologues from *P. buccae*. $[M + Cl]^-$ ions of the ceramide species emerging at 2 to 3 min are shown with ceramide species labelled with a red dot. Determination of the ceramide structures by MS/MS is provided in Extended Data Figs. 7c-d.

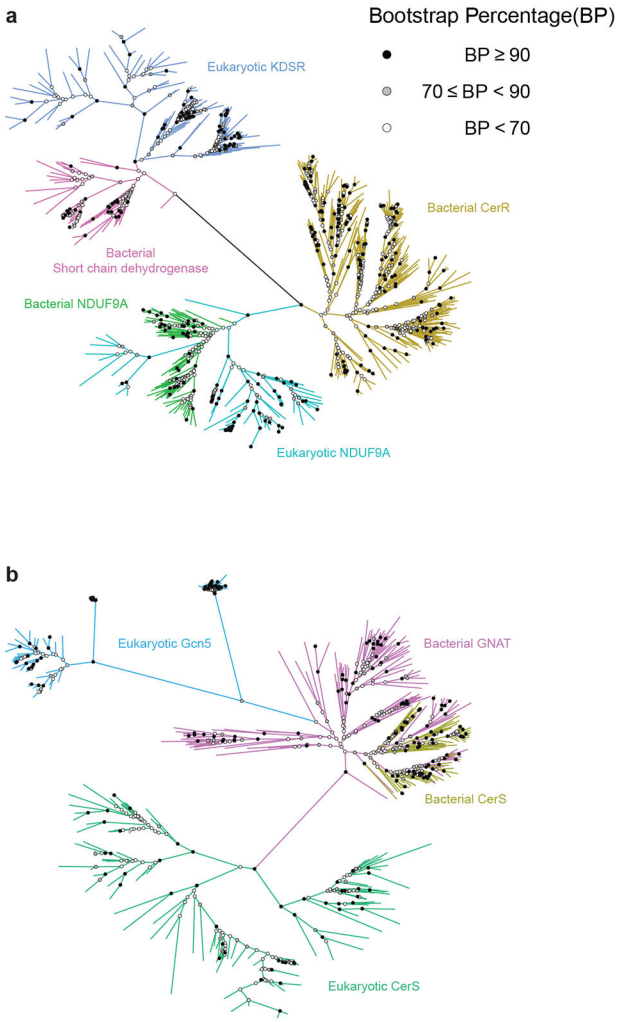

Figure 4. Phylogenetic analysis indicates convergent evolution of ceramide synthesis.

Unrooted trees built using the maximum likelihood method show the distance between eukaryotic and bacterial ceramide synthesis genes as well as their closest homologues. Bootstrap percentage values are indicated by shaded circles at each node. (a) Bacterial CerR is most closely related to eukaryotic and bacterial proteins of the NDUF9A family, a subunit of mitochondrial Complex I. By contrast, Eukaryotic KDSR is homologous to bacterial short-chain dehydrogenases, unrelated to CerR. (b) Bacterial bCerS is part of a larger family of GNAT acyltransferases, which are, in turn closely related to eukaryotic Gcn5 proteins. By contrast, eukaryotic CerS proteins are distant from the Gcn5-related proteins.